

Electronic Structure of Lanthanum Calcium Oxoborate $\text{LaCa}_4\text{O}(\text{BO}_3)_3$

*A.J. Nelson, T. van Buuren, T.M. Willey, C. Bostedt,
J.J. Adams, K.I. Schaffers, L. Terminello, T.A. Callcott*

This article was submitted to
9th International Conference on Electronic
Spectroscopy and Structure
Uppsala, Sweden, June 30 – July 4, 2003

June 26, 2003

U.S. Department of Energy

Lawrence
Livermore
National
Laboratory

DISCLAIMER

This document was prepared as an account of work sponsored by an agency of the United States Government. Neither the United States Government nor the University of California nor any of their employees, makes any warranty, express or implied, or assumes any legal liability or responsibility for the accuracy, completeness, or usefulness of any information, apparatus, product, or process disclosed, or represents that its use would not infringe privately owned rights. Reference herein to any specific commercial product, process, or service by trade name, trademark, manufacturer, or otherwise, does not necessarily constitute or imply its endorsement, recommendation, or favoring by the United States Government or the University of California. The views and opinions of authors expressed herein do not necessarily state or reflect those of the United States Government or the University of California, and shall not be used for advertising or product endorsement purposes.

This is a preprint of a paper intended for publication in a journal or proceedings. Since changes may be made before publication, this preprint is made available with the understanding that it will not be cited or reproduced without the permission of the author.

This report has been reproduced directly from the best available copy.

Available electronically at <http://www.doc.gov/bridge>

Available for a processing fee to U.S. Department of Energy
And its contractors in paper from
U.S. Department of Energy
Office of Scientific and Technical Information
P.O. Box 62
Oak Ridge, TN 37831-0062
Telephone: (865) 576-8401
Facsimile: (865) 576-5728
E-mail: reports@adonis.osti.gov

Available for the sale to the public from
U.S. Department of Commerce
National Technical Information Service
5285 Port Royal Road
Springfield, VA 22161
Telephone: (800) 553-6847
Facsimile: (703) 605-6900
E-mail: orders@ntis.fedworld.gov
Online ordering: <http://www.ntis.gov/ordering.htm>

OR

Lawrence Livermore National Laboratory
Technical Information Department's Digital Library
<http://www.llnl.gov/tid/Library.html>

Electronic Structure of Lanthanum Calcium Oxoborate $\text{LaCa}_4\text{O}(\text{BO}_3)_3$

A. J. Nelson,¹ T. van Buuren,¹ Trevor M. Willey,¹ C. Bostedt,¹ J.J. Adams,¹ K. I. Schaffers,¹
Lou Terminello¹ and T.A. Callcott²

¹*Lawrence Livermore National Laboratory, Livermore, CA 94550 USA*

²*Department of Physics, University of Tennessee, Knoxville, TN 37996*

Abstract

Lanthanum calcium oxoborate (LaCOB) is a nonlinear optical material that belongs to the calcium–rare-earth (R) oxoborate family, with general composition $\text{Ca}_4\text{RO}(\text{BO}_3)_3$ ($\text{R}^{3+} = \text{La}, \text{Sm}, \text{Gd}, \text{Lu}, \text{Y}$). X-ray photoemission, photoabsorption and resonant fluorescence were applied to study the electronic structure and surface chemistry of this material. High resolution photoemission measurements on the valence band electronic structure and La $3d$ and $4d$, Ca $2p$, B $1s$ and O $1s$ core lines were used to evaluate the surface and near surface chemistry. Element specific density of unoccupied electronic states in LaCOB were probed by x-ray absorption spectroscopy (XAS) at the La $3d$ ($M_{4,5}$ -edge), La $4d$ ($N_{4,5}$ -edge), B $1s$ and O $1s$ (K-edges) absorption edges. Soft x-ray fluorescence was used to further examine valence band states associated with spectral differences noted in the absorption measurements. These results provide the first measurements of the electronic structure and surface chemistry of this rare-earth oxoborate.

Introduction

Lanthanum calcium oxoborate (LaCOB) is a nonlinear optical (NLO) material that belongs to the calcium–rare-earth (R) oxoborate family, with general composition $\text{Ca}_4\text{RO}(\text{BO}_3)_3$ ($\text{R}^{3+} = \text{La, Sm, Gd, Lu, Y}$). [1,2] The nonlinear properties of these crystals have been measured and LaCOB is found to have potential for high-average power frequency conversion and intra-cavity doubling. [3]

The optical properties of borate crystals appeared to be related to their molecular structure. These crystals are constructed from a basic structure unit: $(\text{BO}_3)^{3-}$ anionic groups. The anionic group is thought to determine the NLO coefficient of borate crystals according to the anionic group theory [4]. If the dangling bonds of the three terminated oxygen atoms of the $(\text{BO}_3)^{3-}$ groups are interlinked with cations, an absorption edge appearing at wavelengths as short as 155 nm is also possible.

LaCOB crystallizes in the monoclinic biaxial crystal system belonging to the *Cm* space group, and the number of unit formula is $Z = 2$. [5] LaCOB is isostructural to the calcium fluoroborate $\text{Ca}_5(\text{BO}_3)_3\text{F}$, which is related to the common fluoroapatite structure $\text{Ca}_5(\text{PO}_4)_3\text{F}$. [6,7]

There are two types of Ca^{2+} ion that occupy distorted octahedral sites. All octahedra share corners with BO_3 triangles to form a three-dimensional network. There are two kinds of boron site, B(1) and B(2), with threefold coordination. The planar borate unit lies approximately parallel to the (001) plane.

The La^{3+} ions are located in the crystallographic mirror plane (Fig. 1). The environment of La^{3+} ion is a distorted octahedron with *Cs* site symmetry. Four oxygen ions are shared with the BO_3 groups. One should also consider the existence of a probable disorder

between calcium and lanthanum atoms in the two octahedral positions. [5]

This paper presents results from an investigation of the composition and the electronic structure of this rare-earth calcium oxoborate. Core-level spectroscopy and results for the occupied states in the valence band and unoccupied states in the conduction band are the first measurements for this material.

Experimental

The LaCOB compound was prepared by classical solid-state reaction, with La_2O_3 , CaCO_3 , and B_2O_3 in stoichiometric proportions. The mixture was heated at 950 °C for 18 h, cooled and ground, and then heated again at 1350 °C for 24 h. The x-ray diffraction patterns confirmed that the compound was a single phase.

Large crystals of LaCOB, grown by the Czochralski method, were obtained through careful alignment of the seed crystal along the preferred growth direction (the dielectric axis). This material melts congruently, and crystals were grown while rotating at 20 rpm with a pull rate of 1 mm/h from a 7.62-cm diameter iridium crucible. Typical growth sizes were 2.5–3.0 cm diameter x 10 cm in length. The crystals were clear, with minimal bubble core defects perpendicular to the [010] growth direction. The location of the dielectric axis was determined by x-ray diffraction, and 1-mm thick samples were cut for analysis. LaCOB was found to be transparent between 200 and 2400 nm.

X-ray photoemission spectroscopy (XPS) was performed using a focused monochromatic Al K α x-ray (1486.7 eV) source for excitation and a spherical section analyzer. The instrument has a 16-element multichannel detection system. A 1 mm diameter x-ray beam was used for analysis. The x-ray beam is incident normal to the sample and the x-

ray detector is at 45° away from the normal. The pass energy was 23.5 eV giving an overall energy resolution of 0.3 eV. The collected data were referenced to an energy scale with binding energies for Cu $2p_{3/2}$ at 932.72 ± 0.05 eV and Au $4f_{7/2}$ at 84.01 ± 0.05 eV. Surface contamination was removed by sputter etching with 1 kV Ar^+ ions prior to compositional analysis. Low energy electrons and argon ions were used for specimen neutralization.

X-ray absorption spectroscopy (XAS) was performed at beamline 8.2 at the Stanford Synchrotron Radiation Laboratory (SSRL) by scanning the photon energy of the incoming monochromatic synchrotron radiation through the La $3d$ ($M_{4,5}$ -edge), La $4d$ ($N_{4,5}$ -edge), B $1s$ and O $1s$ (K-edges) core-level edges while monitoring the total electron yield (TEY, surface sensitive, 50-100Å).

Soft x-ray fluorescence spectroscopy (SXRF) was performed in conjunction with XAS analysis at beamline 8.0.1 of ALS. It is a bulk-sensitive probe due to the long mean free path of photons in solids (0.1–1.0 μm). Since core levels are involved in absorption and emission, SXRF is both element- and angular-momentum-selective. SXRF measures the local element specific partial density of states (DOS).

In SXRF, a valence emission spectrum results from transitions from valence band states to the core hole produced by the incident photons. In the non-resonant energy regime, the excitation energy is far above the core binding energy, and the absorption and emission events are uncoupled. The fluorescence spectrum resembles emission spectra acquired using energetic electrons and is insensitive to the incident photon's energy. In the resonant excitation energy regime, core electrons are excited by photons to unoccupied states just above the Fermi level. The absorption and emission events are coupled and this coupling manifests itself in several ways depending in part on the localization of the empty electronic

states in the material. This resonant inelastic x-ray scattering (RIXS) near threshold provides not only band structure information, but also provides a clear elucidation of chemical effects in the material.

Results and Discussion

Figures 2(a) and (b) present the high-resolution La $3d_{5/2,3/2}$ and La $4d_{5/2,3/2}$ core-level spectra for the LaCOB crystal and La-oxide model compound, respectively. The La $3d_{5/2}$ and $3d_{3/2}$ spin-orbit peaks are doublets that are indicative of two bonding states. Specifically, for La 3d photoemission, the core-level final state configuration can be either $3d^9 4f^0$ or $3d^9 4f^1 \underline{L}$ due to final state screening effects, where \underline{L} indicates that there is one electron missing in the ligand valence state, i.e. O 2p hole. The doublet structure is due to bonding and antibonding states between the $3d^9 4f^0$ or $3d^9 4f^1 \underline{L}$ configurations. [8] The small energy difference indicates a high degree of mixing between these two states.

The La 4d photoemission also shows the manifestation of the p - f bonding-antibonding states as indicated by the branching ratio of the $4d_{5/2,3/2}$ spin-orbit pair. In addition, multiplet structures due to the La $4d$ - $4f$ interaction are also included in the spectrum envelope. The high binding energy satellite at ~ 109 eV is ascribed to the antibonding state due to O $2p$ -La $5d$ hybridization based on a model proposed for Ce compounds. [9]

The B 1s binding energy from the core-level spectra shown in Figure 3(a) is 193.3 eV for the B_2O_3 , in agreement with the literature. [10,11] The boron in LaCOB exhibits less of a chemical shift and has a B 1s binding energy of 191.2 eV. This can be explained by first noting that each B atom in the LaCOB unit cell is coordinated with three O atoms forming BO_3 triangles in a three-dimensional network at two sites in the LaCOB lattice. However, the

B at these sites shares oxygen with the Ca and La complexes, and the Ca-O bond is predominantly ionic. Thus, the majority of the oxygen charge is shared not with the B, but with the Ca.

Figure 3(b) presents the O 1s core-level spectra for the LaCOB and the model oxide compounds. The binding energy ranges for the oxides are comparable to literature values. [11,12] The full-width-half-maximum (FWHM) of the O 1s peak for the LaCOB is 2.2 eV, and for the La₂O₃ is 2.0 eV. Oxygen is bonded to La, Ca and B in the LaCOB unit cell and thus the larger FWHM is expected. Also, the absence of a strong chemical shift for LaCOB is consistent with the B 1s results.

The valence band (VB) spectra for the LaCOB crystal and model compounds are presented in Figure 4. The upper valence bands are composed primarily of B and O 2*p* states that hybridize with the La 5*d* states. In addition, the unoccupied La 4*f* states that lay approximately 2 eV above E_F, hybridize significantly with these upper valence bands. [13] The higher binding energy La 5*p*, Ca 3*p*, O 2*s* and La 5*s* core-level peaks are also shown in this figure. Note the multiplet splitting of the La 5*s* peak and the branching ratio of the La 5*p*_{3/2,1/2} spin-orbit pair for the LaCOB crystal. These core-level multiplet structures are best understood in terms of configuration-interaction (CI) calculations including intrashell electron correlation, charge-transfer and final-state screening. [14-16] In addition, these multiplet structures are also strongly influenced by covalency and ligand coordination [17], specifically the La³⁺O₆ⁿ⁻ groups.

XAS was used to probe the empty or unfilled electronic states and to provide information on the local chemical environment of the atomic constituents. Specifically, the La 3*d* (M_{4,5}-edge), La 4*d* (N_{4,5}-edge), B 1*s* and O 1*s* (K-edges) absorption edges were measured.

For the La $M_{4,5}$ -edge shown in Figure 5(a), the $3d^{10}4f^0 \rightarrow 3d^94f^1$ transitions dominate, but intermediate states are also allowed under the electric dipole selection rules. [18,19] The creation of an intermediate $3d^94f^1L$ charge transfer state (La $3d$ photoemission final state) is directly related to the Coster-Kronig transition ($3d^{10}5p^64f^0 \rightarrow 3d^95p^64f^1 \rightarrow 3d^{10}5p^54f^1$), which promotes charge transfer with the ligand valence state. For mixing or hybridization to occur, the charge transfer states should have the same symmetry as the initial state. Previous work has shown that the intermediate states are not coupled and the hybridization strength between the $4f$ and valence band is minimal. [18,19] Rather, significant O $2p$ -La $5d$ hybridization is present based on the photoemission results.

In the case of the La $N_{4,5}$ -edge presented in Figure 5(b), the dipole allowed transitions are $4d \rightarrow 4f$ and $4d \rightarrow 5p$, with transitions to the $4f$ states dominant. The super Coster-Kronig transition ($4d^{10}5p^64f^N \rightarrow 4d^95p^64f^{N+1} \rightarrow 4d^{10}5p^54f^{N+1}$) with $4d$ core-excited intermediate states becomes weakly dipole-allowed due to spin-orbit interaction and manifests itself as pre-threshold features. [20-22] Enhancement of these intermediate transitions has been noted when valence electrons associated with oxygen bonding contribute, e.g. the presence of $La^{3+}-O^{2-}$ complexes. [23] Since the ground state of La has an unfilled $4f$ shell, the decay process associated with the $4d$ hole provides information about the character of the $4f$ (and $5p$) wave functions. Unfortunately, the decay process is inherently weak and was not observed with SXRF in this study.

Boron K-edge XAS spectrum for the LaCOB crystal is presented in Figure 6(a). The spectral features reflect transitions to unoccupied p -like states and give a representation of the p -like unoccupied density of states. The principal features identified in the spectrum are the sharp peak at 192.8 eV and the broad peak centered at 201.6 eV. The sharp peak is associated

with trigonal $(\text{BO}_3)^{3-}$ anionic groups and is assigned to the transition from the B 1s core-level up to the unoccupied B $2p_z$ orbital. The broad feature is assigned to the transition from the B 1s core-level to the unoccupied B-O π^* antibonding orbital. [24,25] The $-\text{BO}_3$ is strongly polarized in the lattice due to reduced negative charge around the $(\text{BO}_3)^{3-}$ anionic groups that are interlinked with La^{3+} and Ca^{2+} cations.

Emission spectra excited near the B 1s threshold are presented in Figure 6(b). The resonant enhancement of the upper shoulder in the spectrum excited at 191.92 eV is clear evidence for the presence of the RIXS process in the threshold region. All of the emission spectra excited at energies above about 193 eV are essentially identical and provide a reliable measure of the p -PDOS of filled states at the boron site in LaCOB.

The O K-edge XAS spectrum for the LaCOB crystal is shown in Figure 7(a). The O K-edge is rich in structure arising from O in the $(\text{BO}_3)^{3-}$ and $\text{La}^{3+}\text{O}_6^{n-}$ groups, with little contribution from the predominantly ionic Ca-O bonds. [26] In fact, the features at 541.6 eV and 551.5 eV closely match features in the O K-edge spectrum for H_3BO_3 . Resonant enhancement is not evident in the O 1s emission spectra shown in Figure 7(b). Instead, the emission spectra excited above the K-edge threshold may be cut-off or emission is from the two different oxygen sites in LaCOB.

Conclusions

X-ray photoemission (XPS), photoabsorption (XAS) and fluorescence (SXF) spectroscopy were used to examine the electronic structure of lanthanum calcium oxoborate. XPS results for the occupied states showed a high degree of mixing between the p - f bonding-antibonding states. The valence bands are dominated by B and O $2p$ states that hybridize with

the La $5d$ states and, La $5s$ and $5p$ multiplet splitting was evident. XAS results for the unoccupied states show that both dipole allowed La $3d \rightarrow 4f$ and La $4d \rightarrow 4f$ transitions, and super-Coster-Kronig transitions are enhanced by the presence of $\text{La}^{3+}\text{-O}^{2-}$ complexes. In addition, charge transfer effects were observed at the B $1s$ threshold by resonant inelastic x-ray scattering.

Acknowledgements

We would like to thank the SSRL and ALS staff for their assistance during these experiments. This work was performed under the auspices of the U.S. Department of Energy by University of California, Lawrence Livermore National Laboratory under contract No. W-7405-ENG-48. Work was conducted at the Stanford Synchrotron Radiation Laboratory and the Advanced Light Source at Lawrence Berkeley National Laboratory, which are supported by the U.S. Department of Energy under contract nos. DE-AC03-76SF00515 and DE-AC03-76SF00098, respectively.

References

1. Takatomo Sasaki, Yusuke Mori, Masashi Yoshimura, Yoke Khin Yap, and Tomosumi Kamimura, *Materials Science and Engineering* 30, 1 (2000).
2. R. Norrestam, M. Nygren, and J. O. Bovin, *Chem. Mater.* **4**, 737 (1992).
3. J. J. Adams, C. A. Ebbers, K. I. Schaffers, and S. A. Payne, *Opt. Lett.* **26**, 217 (2001).
4. C. Chen, in: *Laser Science and Technical International Handbook*, Vol. 15, Harwood, New York, 1993.
5. A. B. Ilyukhin and B. F. Dzhurinskii, *Russ. J. Inorg. Chem.* **38**, 847 (1993).
6. Lei Shirong, Huang Qingzhen, Zheng Yifan, Jiang Aidong, and Chen Chuangtian, *Acta Crystallogr. Sect. C* **45**, 1861 (1989).
7. J. G. Fletcher, F. P. Glasse, and A. Howie, *Acta Crystallogr. Sect. C* **47**, 12 (1991).
8. S. Suga, S. Imada, T. Muro, T. Fukawa, T. Shishidou, Y. Tokura, Y. Moritomo and T. Miyahara, *J. Electron Spectroscopy and Related Phenomena* **78**, 283 (1996).
9. M. Takeshige, O. Sakai and T. Kasuya, *J. Phys. Sot. Jpn.* **60**, 666 (1991).
10. Y. Wang, M. Trenary, *Chem. Mater.* **5**, 199 (1993).
11. C.L. Perkins, M. Trenary, T. Tanaka, S. Otani, *Surface Science* **423**, L222 (1999).
12. B. D. Padalia, J. K. Gimzewski and S. Affrossman, W. C. Lang, L. M. Watson and D. J. Fabian, *Surface Science* **61**, 468 (1976).
13. C. G. Olson, P. J. Benning, Michael Schmidt, D. W. Lynch, P. Canfield, and D. M. Wieliczka, *Phys. Rev. Lett.* **76(22)**, 4265 (1996).
14. E.J. McGuire, *Phys. Rev.* **A10**, 13 (1974).
15. J.A. Scarfe, A.R. Law, H.P. Hughes, J.A.C. Bland, G.M. Roe and A.P. Walker, *Phys. Stat. Solidi B* **171**, 377 (1992).

16. B. Hermsmeier, C.S. Fadley, B. Sinkovic, M.O. Krause, J. Jimenez-Mier, P. Gerard, T.A. Carlson, S.T. Manson and S.K. Bhattacharya, *Phys. Rev.* **B48**, 12425 (1993).
17. M. Fujiwara, T. Matsushita and S. Ikeda, *J. Electron Spectroscopy Rel. Phenom.* **74**, 201 (1995).
18. A. Moewes, S. Stadler, R. P. Winarski, D. L. Ederer, M. M. Grush and T. A. Callcott, *Phys. Rev.* **B58**, R15951 (1998).
19. C. Dallera, K. Giarda, G. Ghiringhelli, A. Tagliaferri, L. Braicovich, and N. B. Brookes, *Phys. Rev.* **B64**, 153104 (2001).
20. A. Kotani and S. Shin, *Rev. Mod. Phys.* **73**, 203 (2001).
21. K. Starke, E. Navas, E. Arenholz, Z. Hu, L. Baumgarten, G. van der Laan, C.T. Chen, and G. Kaindl, *Phys. Rev.* **B55(4)**, 2672 (1997).
22. A. Moewes, A. V. Postnikov, E. Z. Kurmaev, M. M. Grush and D. L. Ederer, *Europhys. Lett.*, **49(5)**, 665 (2000).
23. J. Schmidt-May, F. Gerken, R. Nyholm and L.C. Davis, *Phys. Rev.* **B30(10)**, 5560 (1984).
24. T. A. Callcott, L. Lin, G. T. Woods, G. P. Zhang, J. R. Thompson, M. Paranthaman and D. L. Ederer, *Phys. Rev.* **B64**, 132504 (2001).
25. M. E. Fleet and X. Liu, *Phys. Chem. Minerals* **28**, 421 (2001).
26. L. A. J. Garvie, P. R. Buseck, and A. J. Craven, *Canadian Mineralogist* **33**, 1157 (1995).

Figure Captions

- Figure 1. Crystal structure of LaCOB
- Figure 2. XPS core-level spectra for LaCOB crystal and La-oxide model compound (a) La $3d_{5/2,3/2}$ and (b) La $4d_{5/2,3/2}$.
- Figure 3. XPS core-level spectra for LaCOB crystal and oxide model compounds (a) B 1s and (b) O 1s.
- Figure 4. XPS valence band spectra for the LaCOB crystal and the oxide model compounds.
- Figure 5. X-ray photoabsorption spectra for the LaCOB crystal and La-oxide model compound (a) La $M_{4,5}$ -edge and (b) La $N_{4,5}$ -edge.
- Figure 6. (a) B K-edge photoabsorption spectra for the LaCOB crystal and oxide model compound and (b) near threshold fluorescence spectra for the LaCOB crystal.
- Figure 7. (a) O K-edge photoabsorption spectra for the LaCOB crystal and oxide model compound and (b) near threshold fluorescence spectra for the LaCOB crystal.

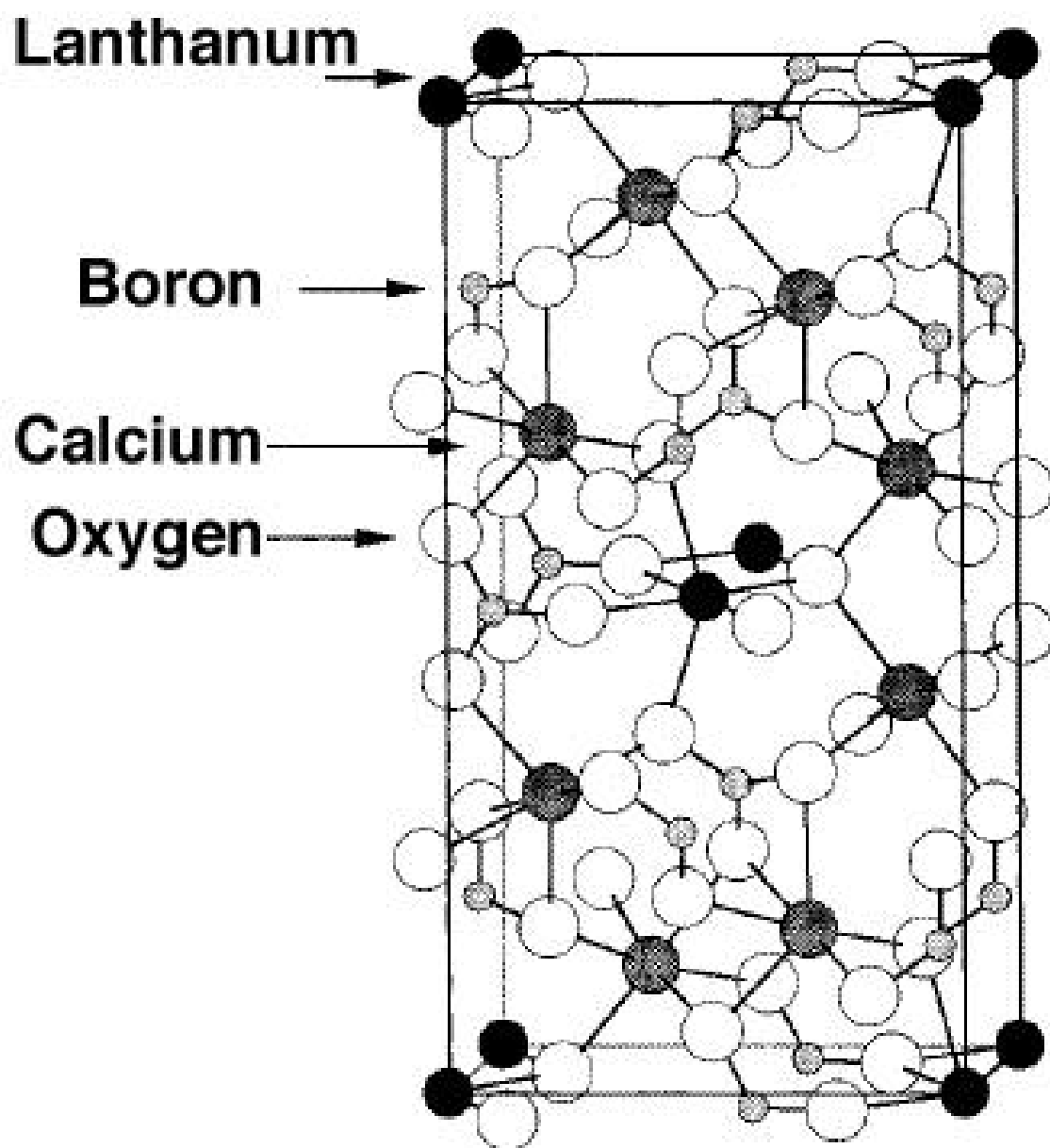


Figure 1.

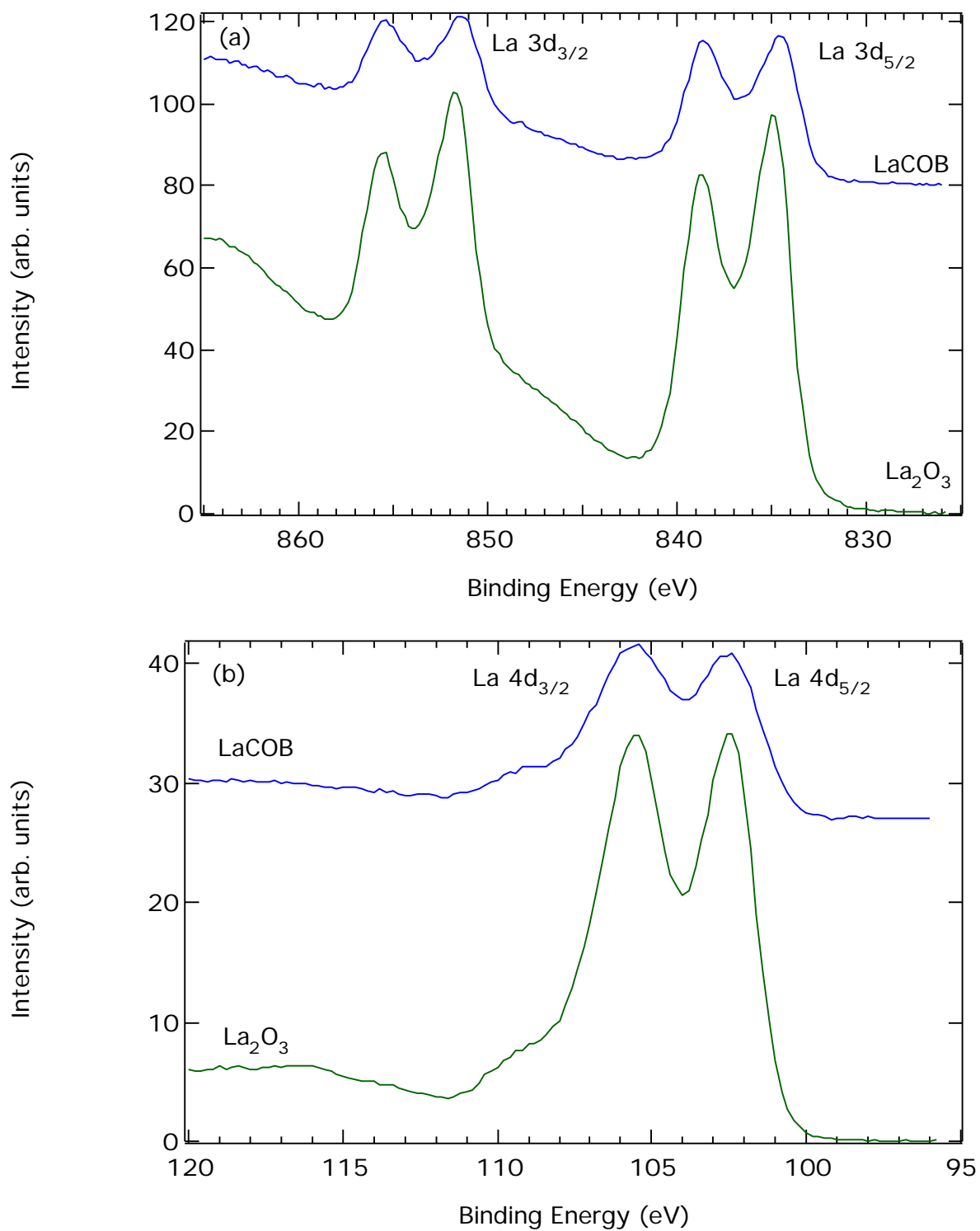


Figure 2.

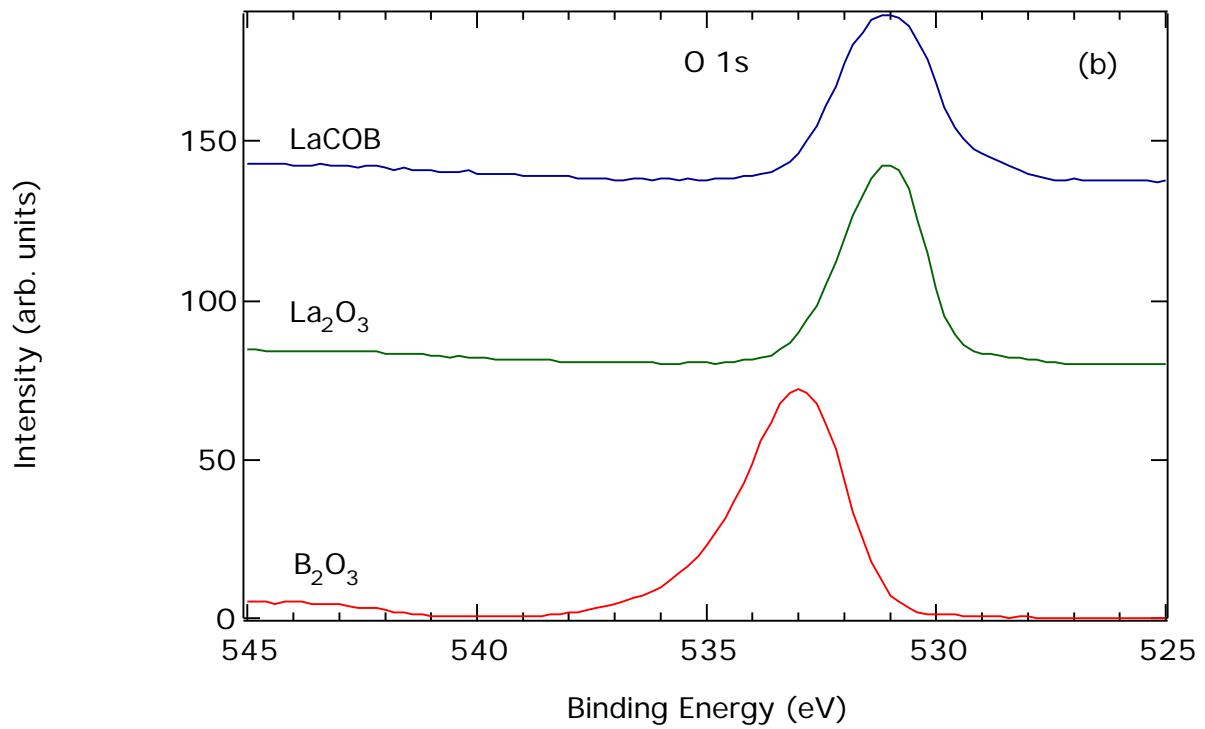
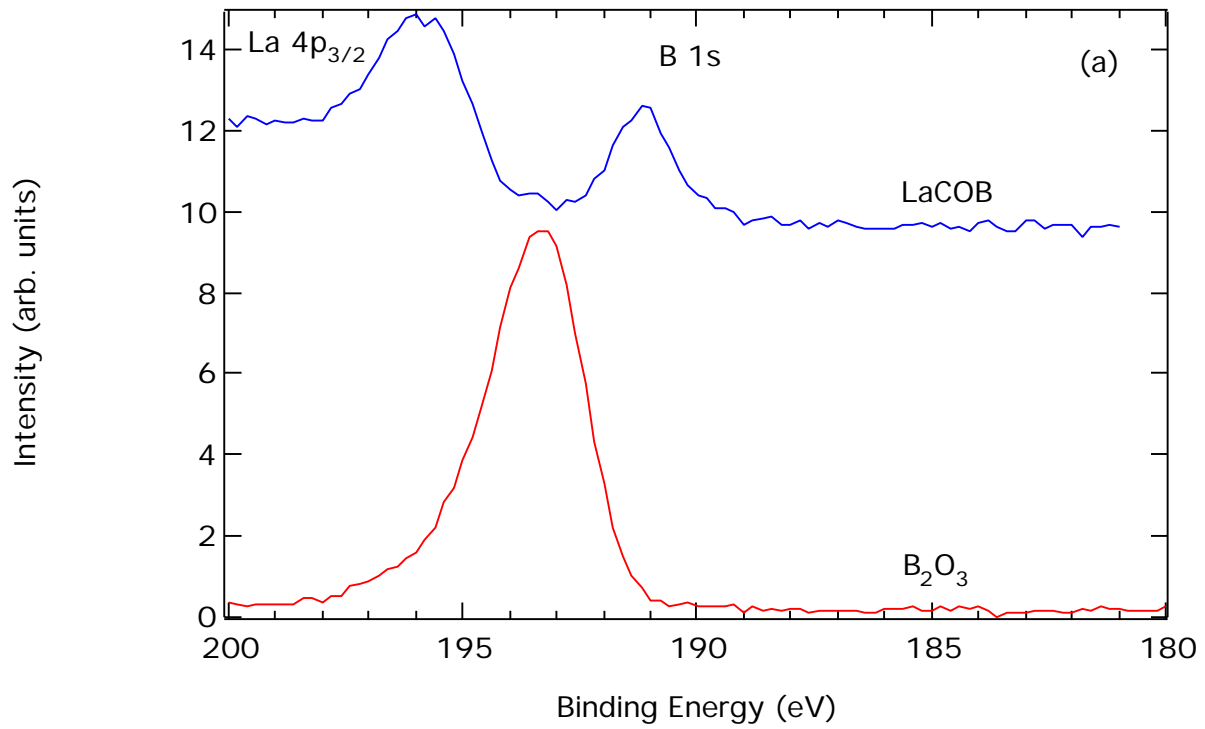


Figure 3.

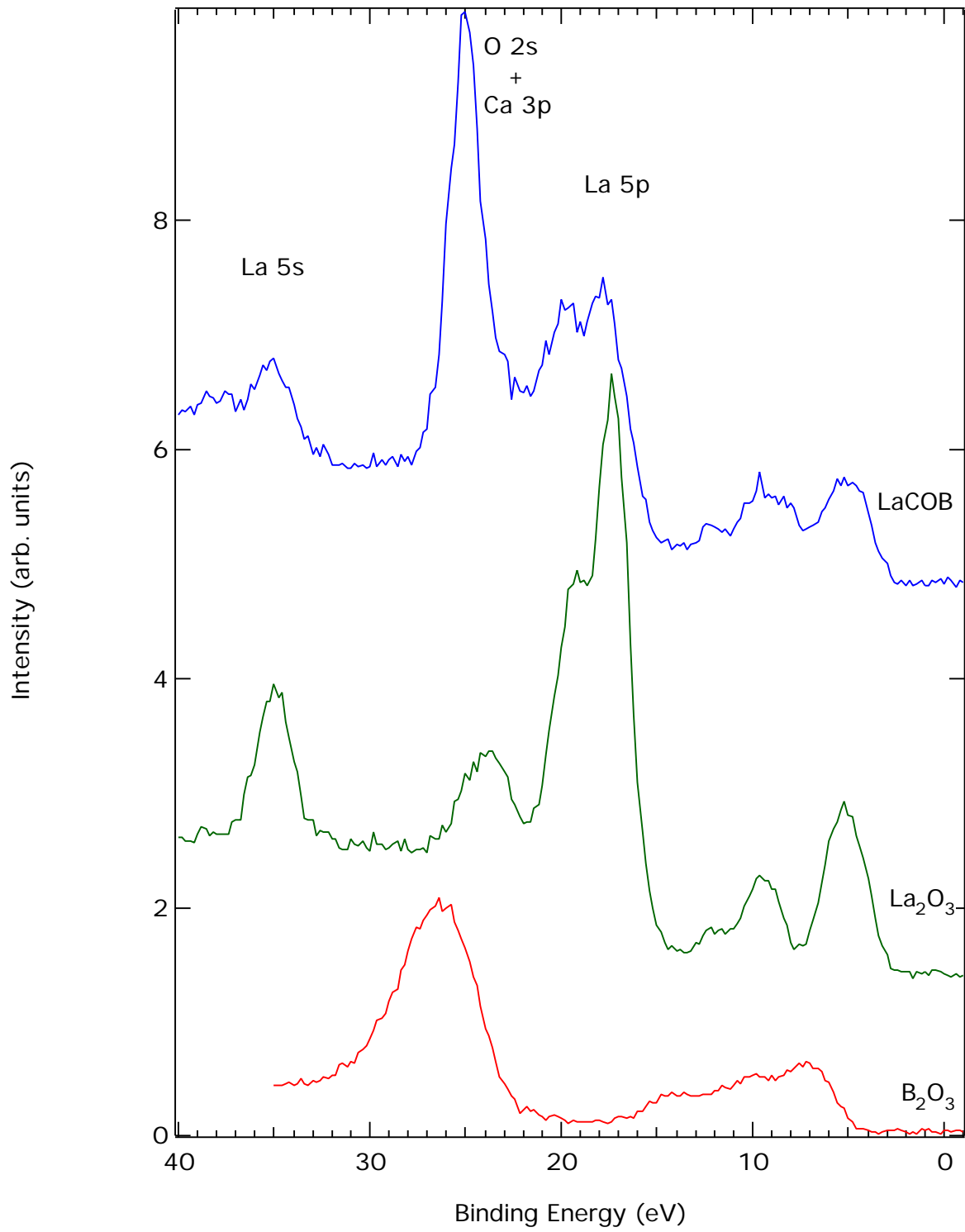


Figure 4.

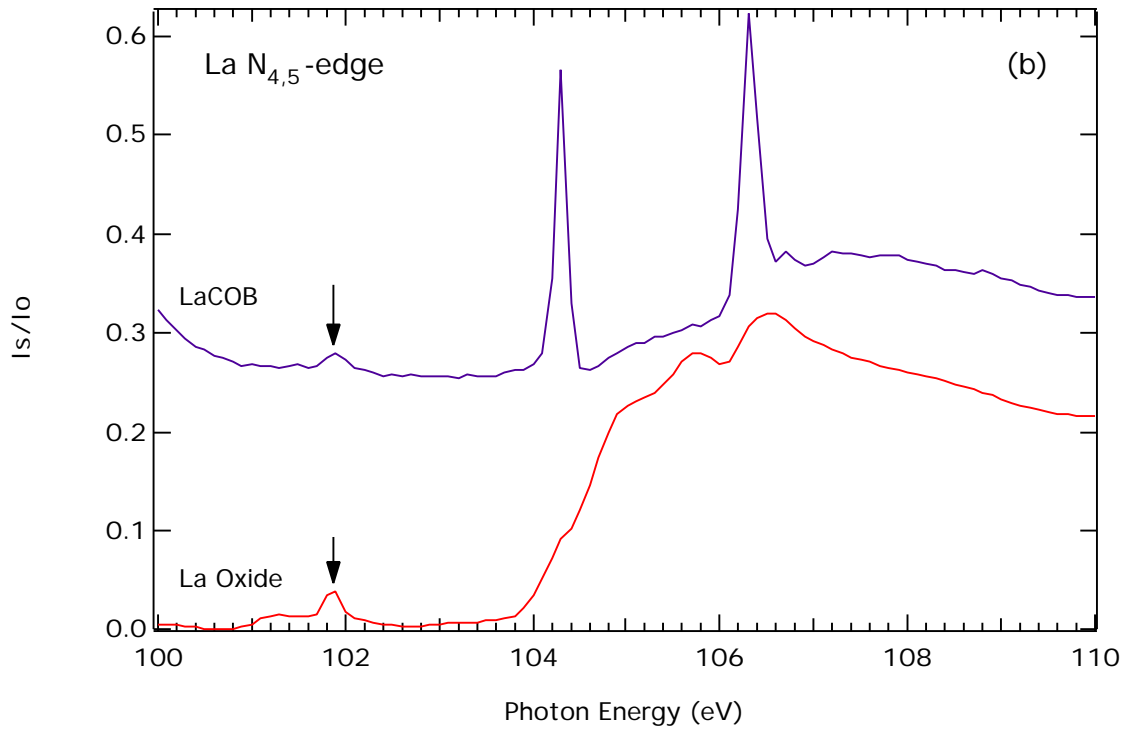
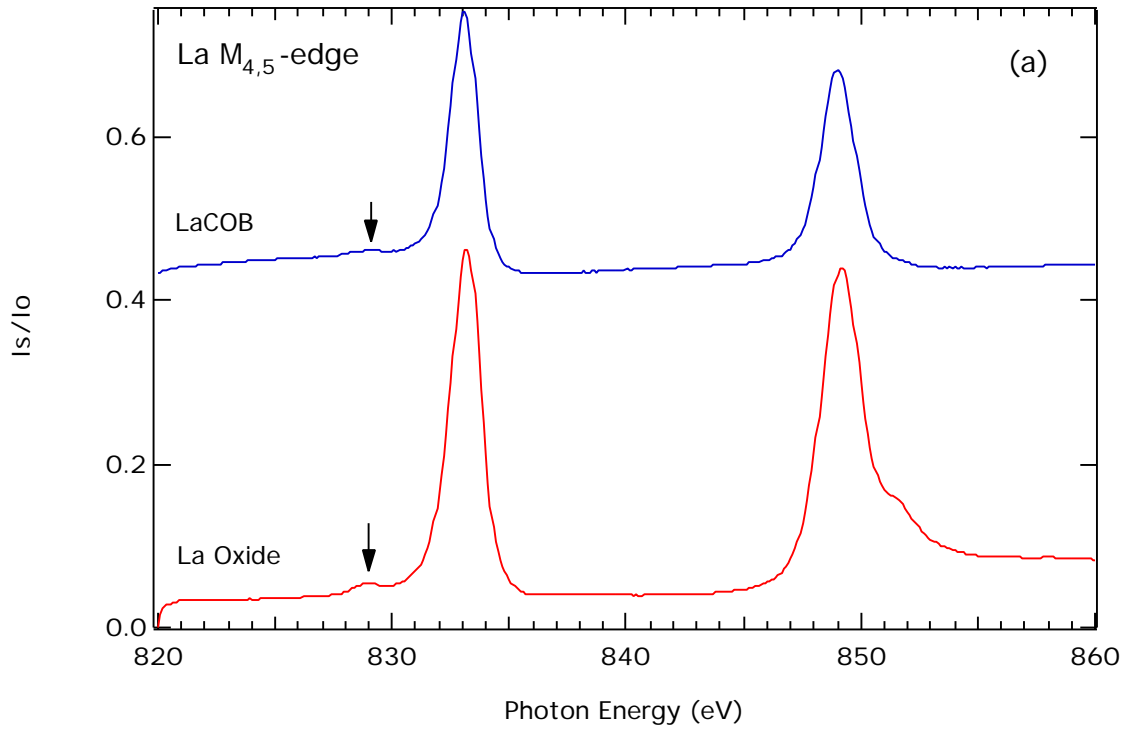


Figure 5.

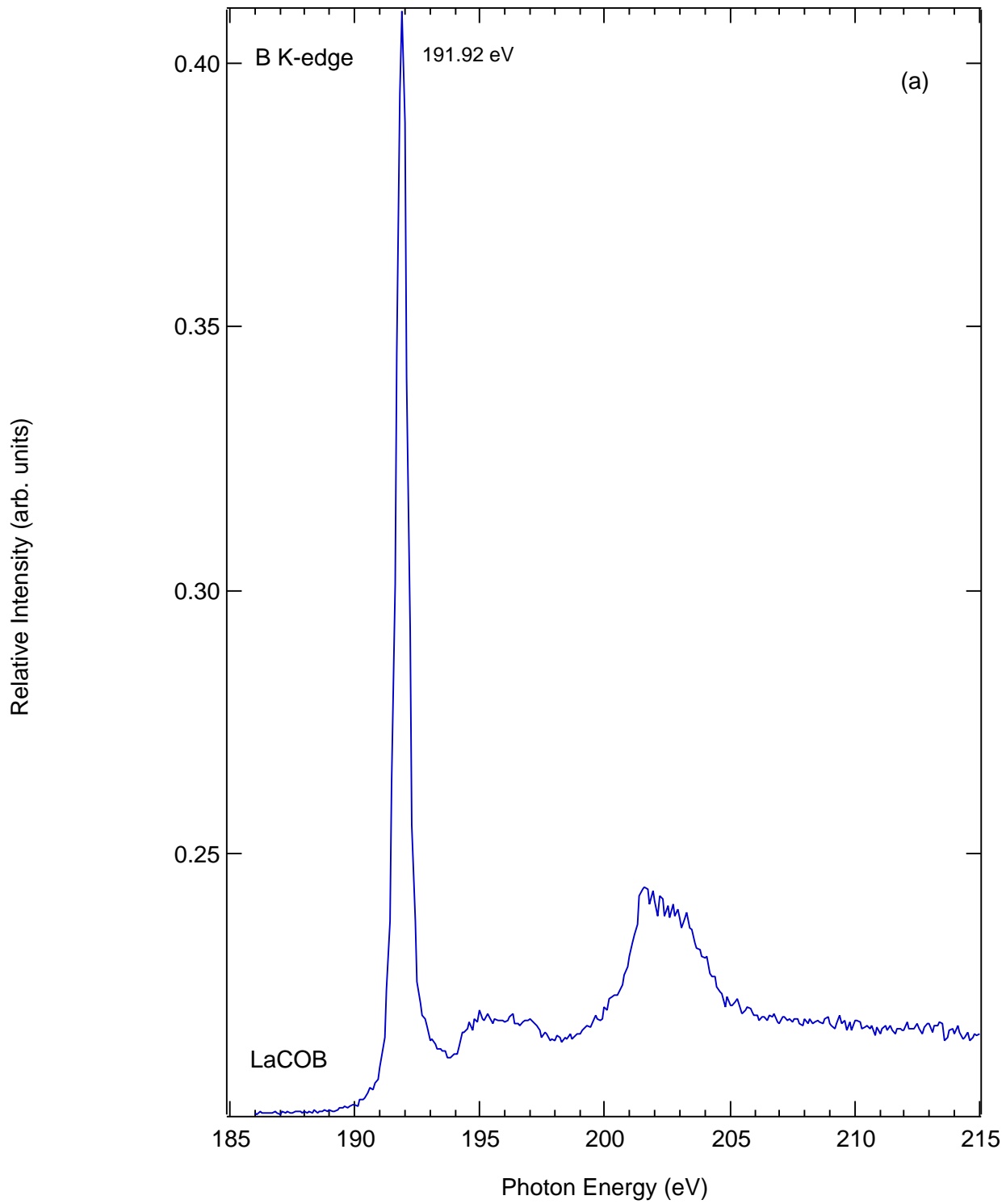


Figure 6(a).

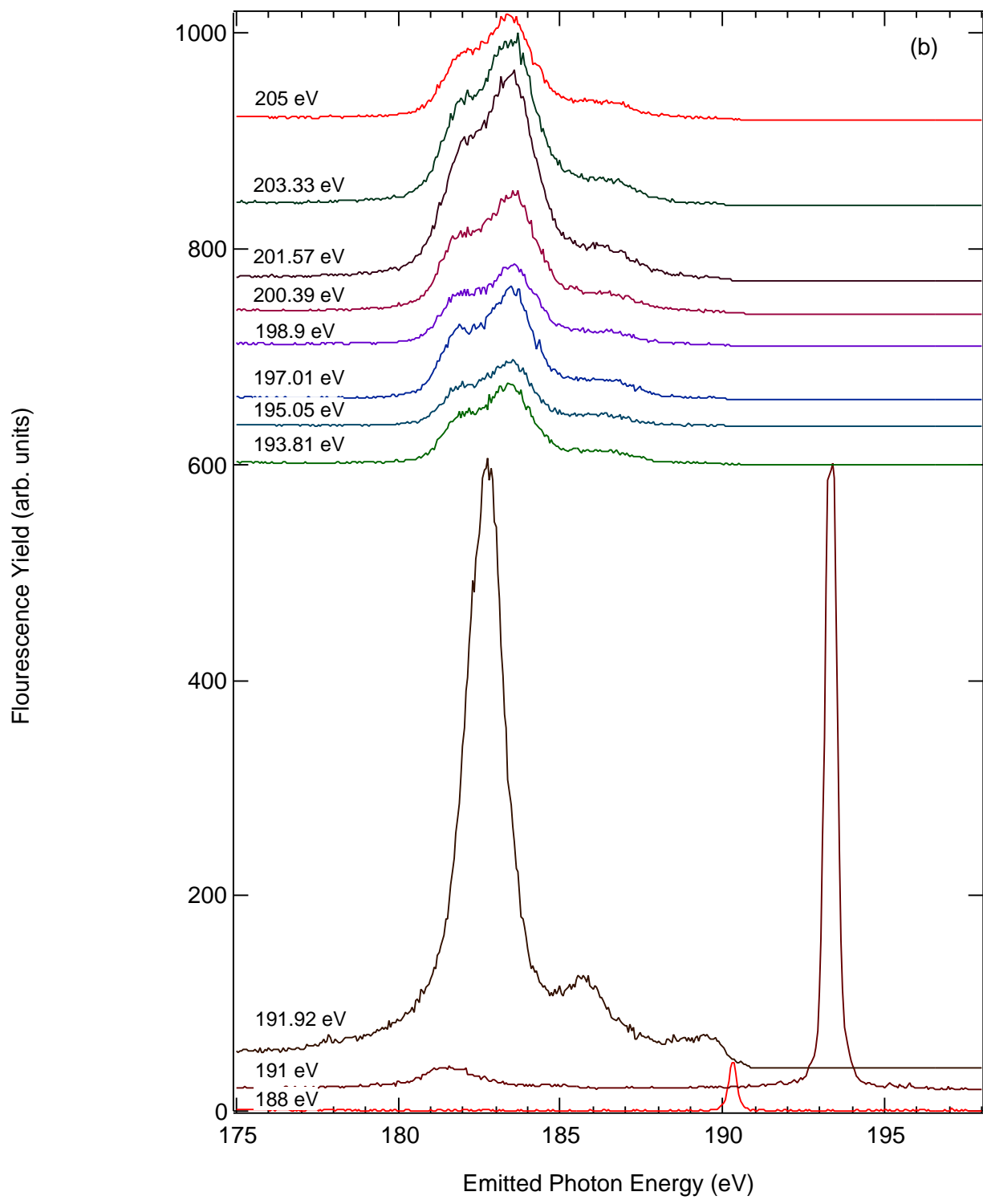


Figure 6(b).

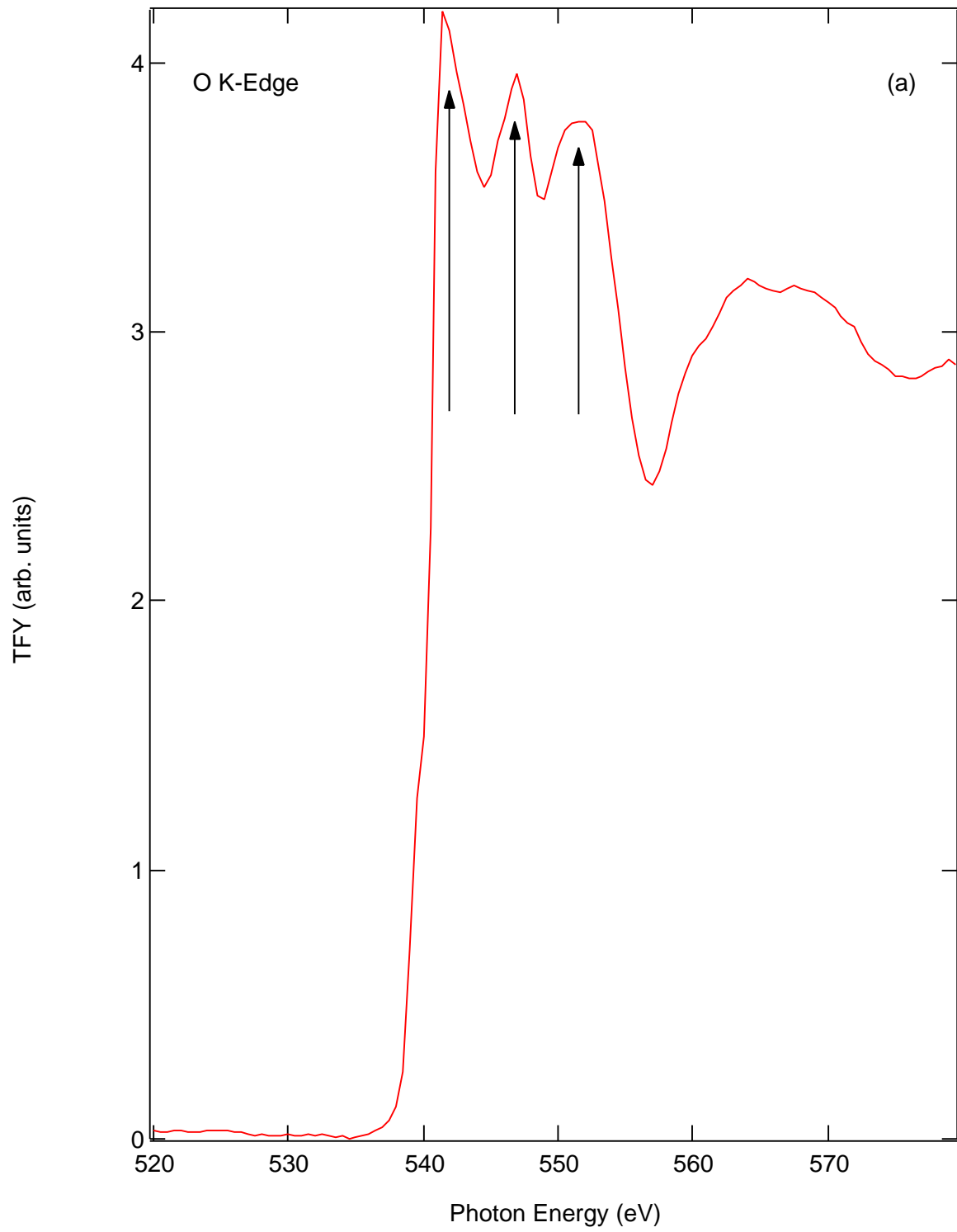


Figure 7(a).

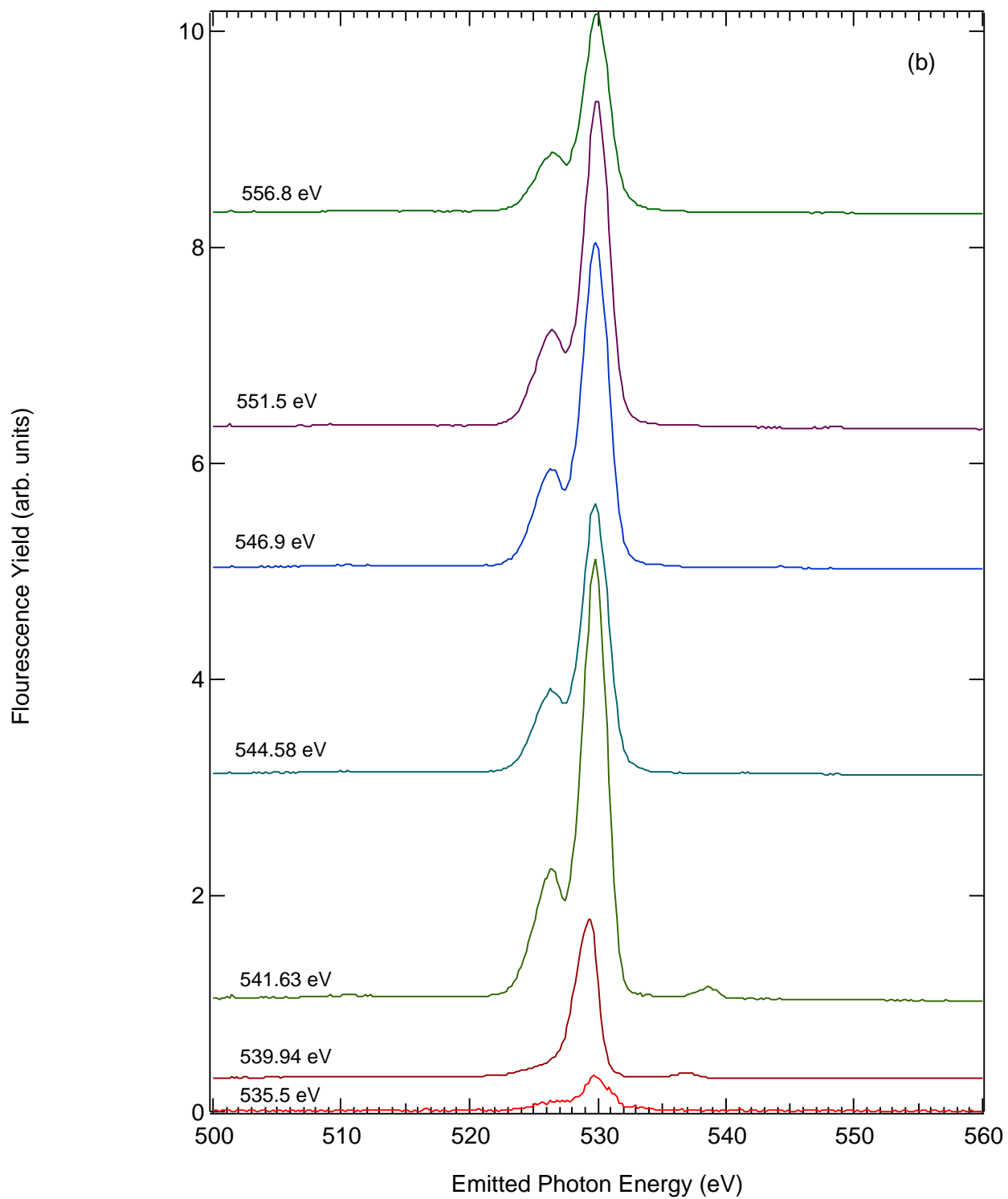


Figure 7(b)